Flow Turbulence Combust (2007) 78: 1–15
DOI 10.1007/s10494-006-9017-7

Self-sustained oscillations of a confined impinging jet

D. Varieras · P. Brancher · A. Giovannini

Received: 5 November 2004 / Accepted: 10 March 2006 /
Published online: 20 September 2006

Abstract The present paper investigates the dynamics of a laminar plane jet impinging on a flat plate in a channel. An experimental parametric study is carried out to determine the flow regimes at different levels of confinement and Reynolds numbers. For very confined jets, the flow is steady whatever the Reynolds number. The overall structure of the flow is symmetric with respect to the jet axis and is characterized by the presence of recirculation zones at the channel walls. The dynamics is radically different for less confined jets. Above a critical Reynolds number, the flow bifurcates in the form of an oscillating flapping mode of the impinging jet. Analyses of the experimental results provide with a quantitative characterization of this regime in terms of amplitude, wavelength and frequency. This self-oscillating bifurcated flow induces strong sweepings of the target plate by the jet and intense vortex dipole ejections from the impacted wall. Such a regime is expected to be particularly useful in the enhancement of the local heat transfer at relatively low cost in terms of flow rate.

Keywords Impinging jet · Global oscillations · Wall heat transfers · Flapping jet · Vortex dipoles · Experimental visualizations

1. Introduction

Jet flows are ubiquitous in industrial applications particularly when intense and controlled transfers are desired. The quantities carried by the flow are usually the temperature or the mass fraction of species. For applications dependent on convective heat transfer, optimization of the thermal performance for a given flow rate of the cooling fluid is crucial. More particularly, impinging jets act on a target wall via strong aerothermal, even acoustic, constraints

D. Varieras · P. Brancher (✉) · A. Giovannini
Institut de Mécanique des Fluides de Toulouse, Allée du Pr. Camille Soula, 31400 Toulouse, France
e-mail: brancher@imft.fr

D. Varieras
Centre de Thermique de Lyon, 20 avenue Albert Einstein, 69621 Villeurbanne cedex, France

concerning the temperature and velocity levels. Among the most common applications, one can cite the cooling of glass surfaces at the exit of the furnace where one seeks the most uniform cooling with an imposed quenching kinetics designed to avoid too strong thermo-mechanical stresses; local cooling of power electronic components or structures with multiple coatings in the presence of large internal dissipation. This last application is in constant development due to the increasing compactness and load of current multiprocessor computers. In aeronautics, the cooling of combustion chambers and the injection of dilution air generate an optimal exit profile of temperature. Moreover impinging jets are often used for the cooling of turbine blades in the same way as turbulence promoters. Finally plane impinging jets are also used to control thickness in thin film coating and to dry wood pulp via mass transfer.

It is generally admitted [1] that the impact of an isolated jet enhances the local transfer an order of magnitude more than classical wall boundary layers. However, the effects are very heterogeneous since the dimension of the impact print is of the same order of magnitude as the characteristic length of the jet for short impacts (i.e. ratios distance from impact over jet thickness less than ten).

A exhaustive bibliographical review reveals that many numerical as well as experimental studies have been dedicated to impinging jet flows. An attempt of classification is presented in [2] following the jet geometry (circular, rectangular or plane cross-section), the confining aspect ratio H/e (where H is the distance from the jet exit to the wall and e the jet thickness), the nature of the impacted surface (plane, inclined or with obstacles), the Reynolds number at the jet exit $\mathrm{Re}_j = U_j e/\nu$ (U_j is the mean jet velocity and ν the kinematic viscosity), the number of impinging jets and the influence of a cross-flow. In the following, the review is restricted to the case of a plane jet impinging on a wall.

Beltraos and Rajaratnam [3] measured the velocity and pressure distributions for a turbulent impinging plane jet in the range $14 < H/e < 70$ and $5270 < \mathrm{Re}_j < 9400$. Ojha and Gollakota [4] carried out numerical simulations to study the influence of the curvature of the target wall on transfer. Striegl and Diller [5] characterized the entrainment and the wall transfer by heat flux measurements for $6 < H/e < 25$. In Chuang [6] numerically investigated the range $2 < H/e < 12$ and $100 < \mathrm{Re}_j < 11000$. For $H/e = 2$ and small Reynolds numbers, he observed a recirculation zone under the impact. This phenomenon disappeared when the advective terms were stronger. His work mainly focused on the pressure distribution on the target wall. The numerical study of Al Sanea [7] compared the respective dynamics of the free jet, the impinging jet and the jet with cross-flow. More recently, Lin et al. [8] proposed an experimental study with $H/e < 8$ in order to quantify the effect of the transition of the jet on heat transfer. Finally, Giang [9] carried out numerical simulations of the unsteady dynamics of laminar and turbulent impinging jets and observed a flapping mode of oscillation.

Though impinging round jets have been extensively studied, it appears that relatively few studies exist on the case of an isolated plane jet impinging in a highly confined configuration ($H/e = 2$ to 9) for laminar and transitional flow regimes ($100 < \mathrm{Re}_j < 1000$). The experimental work exposed in the present paper was carried out in order to get new insights on this configuration. Section 2 describes the experimental setup and the measurement techniques. Visualizations and quantitative measurements are given and analyzed in Sections 3 and 4. They reveal a flow regime characterized by global self-sustained oscillations of the impinging jet above a critical Reynolds number depending on the aspect ratio H/e. Finally a discussion on the physical mechanisms involved is proposed in Section 5.

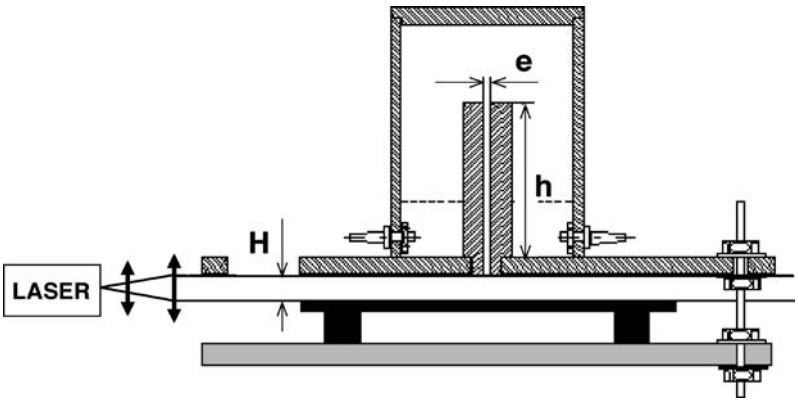

Fig. 1 Experimental setup

2. Experimental setup

2.1. Test bed

The experimental setup is sketched on Figure 1. It is composed of two vertical plates $e = 5$ mm apart and $h = 20$ cm high, such as to generate a parabolic velocity profile at the jet exit. These plates are embedded in a tank supplied by air whose flow rate is controlled and regulated so as to fix the Reynolds number at the jet exit $\mathrm{Re}_j = U_j e/\nu$ (U_j is the mean jet velocity and ν the air viscosity). Incense smoke is generated in the tank for visualizations. The top and bottom horizontal plates confining the flow have dimensions (14 cm $\times$ 35 cm) large enough to confer a quasi-bidimensionnal character on the flow. The vertical gap H can be adjusted by four screws. Therefore this experimental setup allows to fix independantly the two control parameters of the flow, namely the impinging jet Reynolds number $\mathrm{Re}_j = U_j e/\nu$, between 100 and 1000, and the aspect ratio H/e for values between 2 and 10. Further details on the experimental setup can be found in [2] and [10].

2.2. Measurement techniques

2.2.1. Visualizations

The beam generated by a Spectra-Physics 4 Watt-Argon laser is converted into a vertical sheet by a set of cylindrical and spherical lenses. Incense smoke is injected as a tracer. The initial sowing is homogeneous and composed of very small particles so the iso-luminosity (and the iso-concentration) lines can be assimilated to the instantaneous streamlines. A fast Kodak Ektapro EM camera is coupled with a dynamic image analyzer. The acquisition rate is fixed at 125 Hz.

2.2.2. Hot-wire anemometry

The acquisition line is composed of straight and bent probes (Dantec 55P01 and Auspex Co.), a multitrack anemometer (AA Lab System) and an acquisition card on a PC computer using TestPoint. This set and the associated calibration wind tunnel allow measurements in the range of the jet velocities (0.1 to 4 m/s).

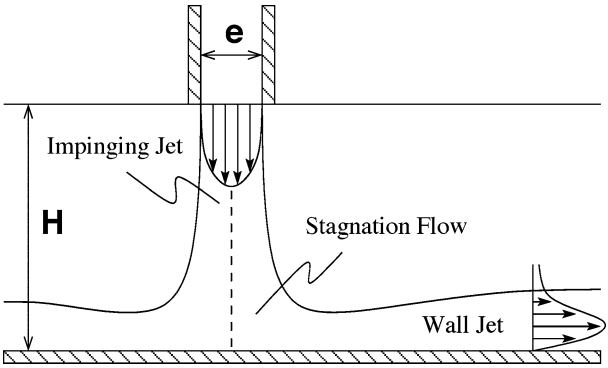

Fig. 2 The three characteristic zones of the flow

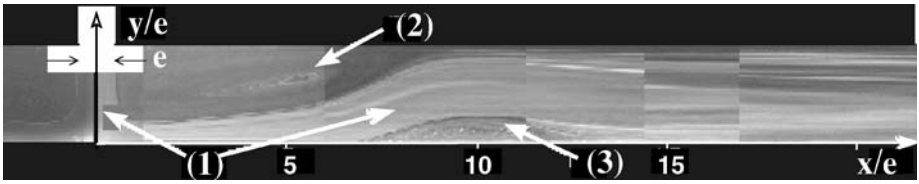

Fig. 3 Flow visualization for $H/e = 2$ at $\mathrm{Re}_j = 120$: jet flows (1), primary (2) and secondary (3) recirculation zones

3. Experimental results

As proposed by Martin [1], the impinging jet flow can be decomposed into three different zones: the emerging jet, the stagnation zone and the wall jet (Figure 2). The experimental results consist of instantaneous laser induced visualizations for different Reynolds numbers and aspect ratios H/e. Velocity measurements provide with the base flow velocity profile in the different zones for steady regimes or the temporal signal at a fixed point in the vicinity of the emerging jet or the wall jet in order to characterize the oscillating regime.

3.1. $H/e = 2$

Figure 3 presents a visualization of the flow for $H/e = 2$ and $\mathrm{Re}_j = 120$. Entrainment by the wall jet is very important and the thickening of the wall jet towards the top plate creates a first recirculation zone above the wall jet. The affine solution in laminar regime gives the following evolution for the jet thickness b:

$$\frac{b}{x} = \frac{\eta}{\sqrt{Ux/\nu}} \tag{1}$$

where η is the Blasius variable of similitude. The order of magnitude of η is 10, and an estimation of the recirculation length x_r such that $b(x_r) = H$ writes (under the assumption that $U \sim U_j$):

$$\frac{x_r}{H} = \frac{H}{e}\frac{\mathrm{Re}_j}{\eta^2} \tag{2}$$

Table 1 Recirculation length vs. Reynolds number for $H/e = 2$

Re_j	x_r/H
120	3.75
220	7.5
350	12

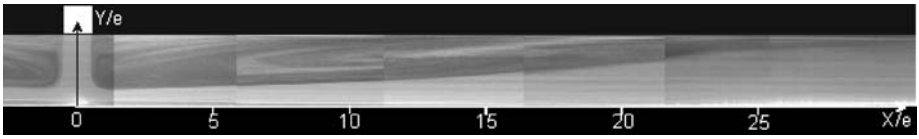

Fig. 4 Flow visualization for $H/e = 2$ at $\mathrm{Re}_j = 350$

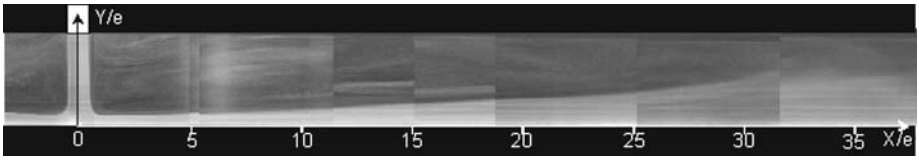

Fig. 5 Flow visualization for $H/e = 4$ at $\mathrm{Re}_j = 350$

This linear evolution with the Reynolds number is confirmed by the experimental results of Table 1.

For $\mathrm{Re}_j = 120$, the adverse pressure gradient generated by the first recirculation zone and the weak inertia of the wall jet induce an upthrust of the latter towards the top wall and the formation of a recirculation lens on the bottom wall.

For higher Reynolds numbers (Figure 4) the wall jet inertia is stronger and the secondary recirculation zone does not exist anymore. For this aspect ratio we observe that the impinging jet is stable for Reynolds numbers between 120 and 610 though wall jet instabilities are observed for $\mathrm{Re}_j > 350$. Nevertheless the whole configuration stays symmetric with respect to the emerging jet axis.

3.2. $H/e = 4$

For $H/e = 4$, we still observe the three zones described by Martin, with a weaker recirculation zone than for smaller aspect ratios (Figure 5). No secondary recirculation zone at the bottom wall is present whatever the Reynolds number. As for the previous aspect ratio, the emerging jet does not develop any instability whereas the wall jet is rapidly unstable.

3.3. $H/e = 8$

For $H/e = 8$ and $\mathrm{Re}_j = 150$ (Figure 6) the emerging jet is still stable while the wall jet develops its inflexional instability. The quantification of the frequency and nature of this instability will be discussed in 5.1. The velocities in the recirculation zone above the wall jet are found to be very weak. Above a critical Reynolds number $\mathrm{Re}_j^c \sim 200$ the impinging jet becomes unstable and develops a sinuous oscillatory mode. Figure 7 shows a complete period of oscillation for $\mathrm{Re}_j = 220$ with a 62.5 image/s rate.

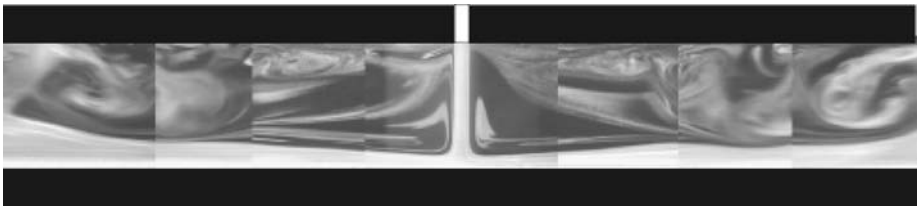

Fig. 6 Flow visualization for $H/e = 8$ at $\mathrm{Re}_j = 150$

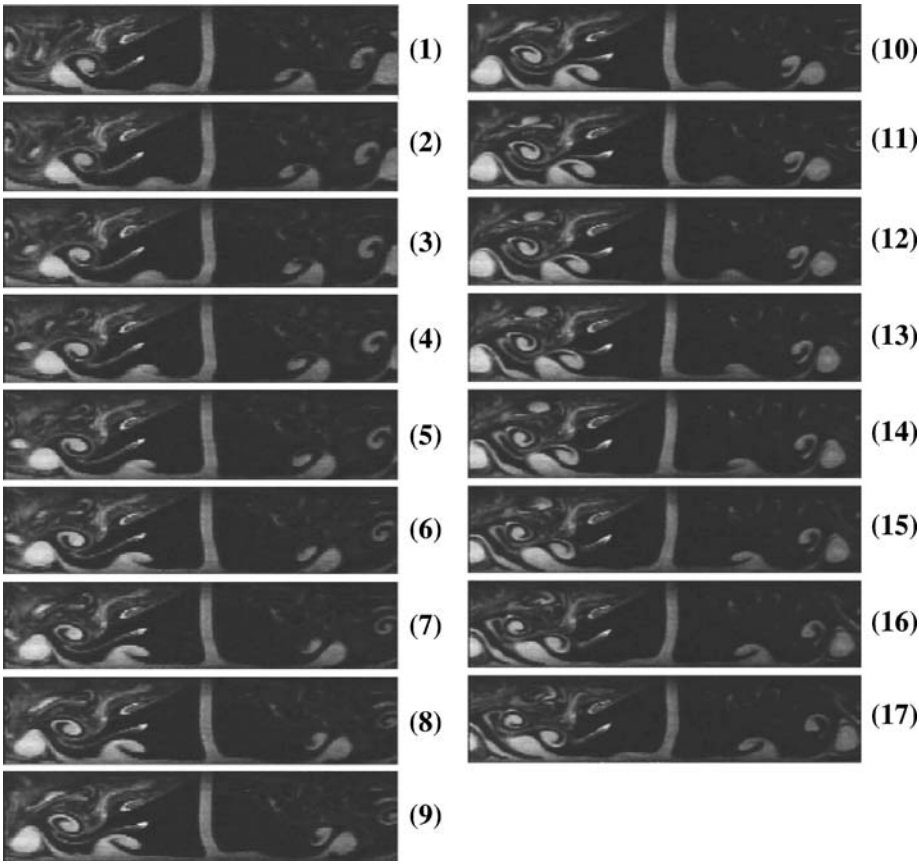

Fig. 7 Flow visualization for $H/e = 8$ at $\mathrm{Re}_j = 220$

One can observe on image (1) the birth of a vortical zone generated by the jet vorticity in the vicinity of the stagnation point. Later (images 2 and 3) a counterrotating vortex originates under the first one by viscous interaction with the bottom wall. The curvature of the jet is still turned towards the vortex dipole thus created. If one considers the dipole trajectory via the velocities induced by one structure to the other, the resulting path is rectilinear which means that the two vortices have similar strength in module. This mechanism is classically called dipolar ejection. It is known to dramatically enhance the momentum, heat and mass transfers. From image (4) the wall jet is nearly cut from the left-hand side of the emerging

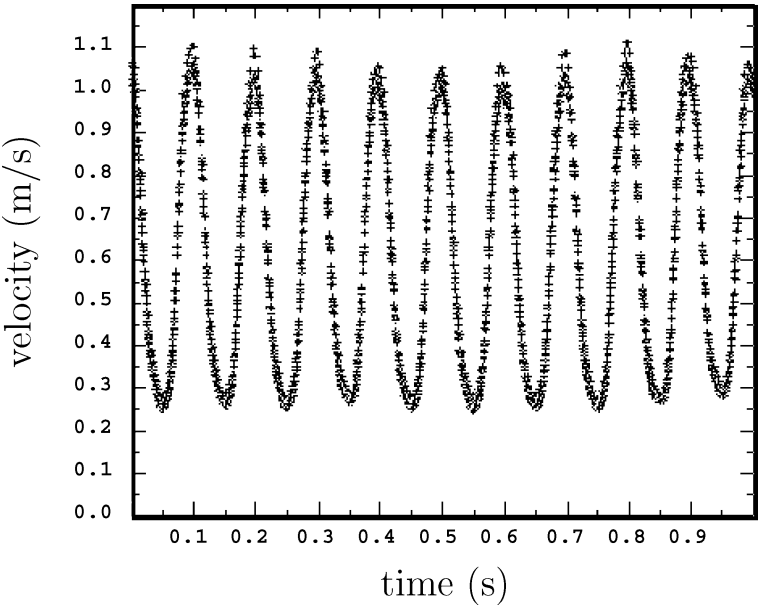

Fig. 8 Velocity fluctuations for $H/e = 8$ at $\mathrm{Re}_j = 220$

Table 2 Oscillations frequency vs. Reynolds number for $H/e = 8$

Re_j	f (Hz)
220	9
340	15
480	21

jet, and the same phenomenon happens alternatively on the right-hand side with respect to the unperturbed emerging jet axis. In order to quantify the frequency of these oscillations, a hot-wire probe was placed in the emerging jet (Figure 8).

Table 2 gives the frequencies measured by analyzing the velocity signals. This flow regime is radically different from the ones encountered for $H/e = 2$ and 4: a sinuous instability leads to an oscillatory motion of the emerging jet at low frequency, thus creating a sweeping of the impacted wall with periodic dipole ejections alternatively on the left and right-hand sides of the impact.

We conclude this phenomenological section by pointing out the determining role played by the aspect ratio H/e on the global dynamics of the flow. For $H/e = 8$, the stable regime at low Reynolds numbers hands over a intermediate regime where the wall jet is subjected to local instabilities. Above a critical Reynolds number, the impinging jet is receptive to fluctuations induced by the wall jet and global self-sustained oscillations develop. This oscillatory mode manifests itself by a sinuous, flapping motion of the emerging jet, a sweeping of the impacted surface, the generation and ejection of vortex dipoles. The following sections characterize in more details the onset of these oscillations and the subsequent time periodic regime.

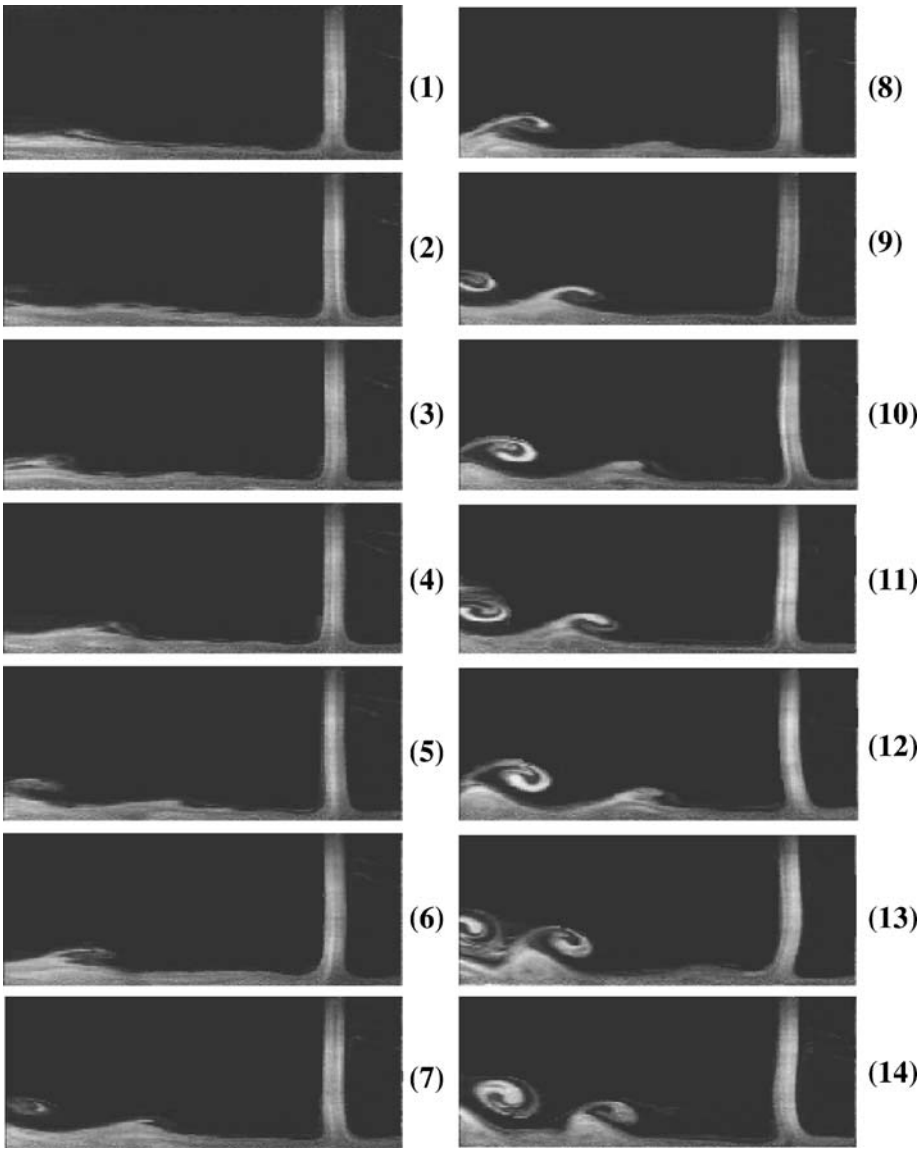

Fig. 9 Visualization of the onset of the oscillations for $H/e = 8$ at $\mathrm{Re}_j = 220$

4. Characterization of the oscillating regime

4.1. Transient regime

The experimental observations of the transient regime were conducted according to the following protocol: from a subcritical Reynolds number at a given aspect ratio (here $H/e = 8$), the flow rate is increased by a few percents above the critical value. The image series of Figure 9 shows the onset of the jet oscillations for $\mathrm{Re}_j = 220$ at a rate of 12.5 images/s.

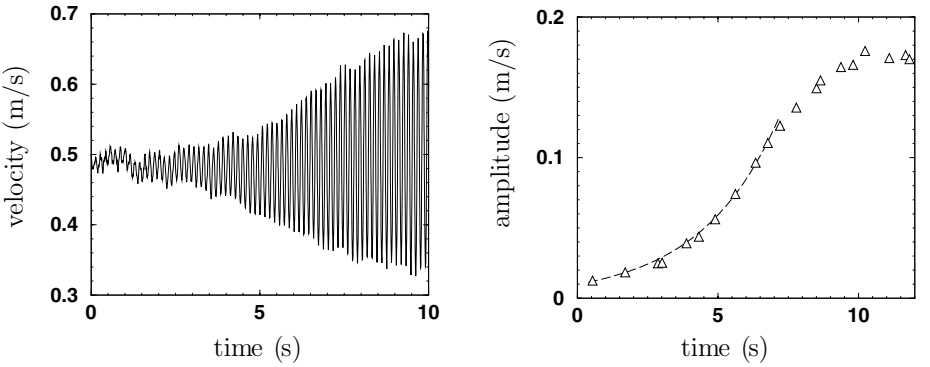

Fig. 10 Time evolution of the velocity signal (a) and its amplitude (b) during the onset of the oscillations for $H/e = 8$ at $\mathrm{Re}_j = 220$

The first images (1–4) show that the emerging jet remains relatively steady whereas the wall jet develops local instabilities. Then the emerging jet begins to destabilize (5–7) before sustaining the formation of dipoles alternately on the right and left-hand sides of the impact (8–14).

Figure 10 shows the time evolution of the velocity signal and its amplitude measured next to the impact in the impinging jet. The amplitude grows exponentially then saturates at $t = 10$ s: the oscillating regime can be analyzed as the result of a global instability of the flow, characterized by a growth rate in the linear regime and a global frequency in its nonlinear saturated state.

4.2. Periodic regime

A parametric study has been carried out in order to quantify the bifurcated oscillatory flow. Figure 11(a) presents the evolution of the critical Reynolds number Re_j^c as a function of the aspect ratio H/e. For H/e smaller than 5 the oscillatory regime has not been observed within the range of Reynolds numbers allowed by our experiment. For $H/e \geq 5$ the critical Reynolds number decreases with increasing H/e. Extrapolation of the neutral curve for small H/e tends to show that $H/e \sim 4.5$ is actually the upper limit of the unconditional stability of the flow with respect to the flapping mode. Figure 11(b) displays the evolution with Re_j of the Strouhal number based on the jet thickness $\mathrm{St}_j = fe/U_j$, where f is the frequency of the global oscillations. For a given aspect ratio, the Strouhal number is approximately constant, which indicates that the frequency could scale with the jet velocity U_j. On the other hand the Strouhal number decreases with increasing aspect ratio H/e.

These observations suggest an alternative choice for the characteristic length scale: if the vertical gap H of the channel is preferred to the jet thickness e, the resulting definitions for the Reynolds number $\mathrm{Re}_H = U_j H/\nu$ and for the Strouhal number $\mathrm{St}_H = fH/U_j$ lead to a noticeably simpler description of the oscillatory regime. As shown on Figure 12(a), the rescaled critical Reynolds number Re_H^c decreases rapidly from $H/e = 5$ before reaching a limit value from $H/e = 7$ onwards. This behaviour allows to conjecture that the flow could be unconditionally stable for $\mathrm{Re}_H < 1600$ whatever the aspect ratio H/e. More radically this new scaling shrinks the scattered results of Figure 11(b) into one single value of the rescaled Strouhal number $\mathrm{St}_H \sim 0.45$ whatever the aspect ratio and Reynolds number. This shows

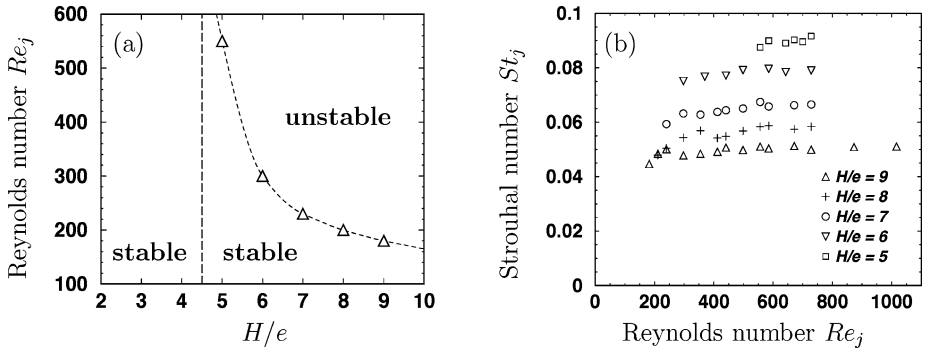

Fig. 11 Critical Reynolds number Re_j^c vs. aspect ratio H/e (a). Strouhal number St_j of the oscillating regime for different aspect ratios (b)

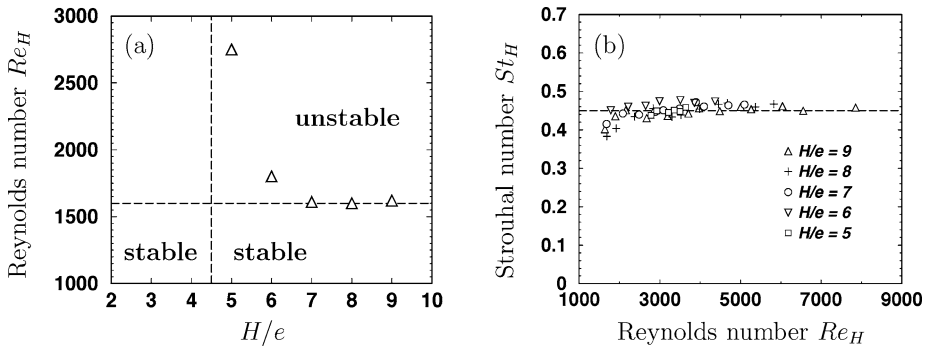

Fig. 12 Critical Reynolds number Re_H^c vs. aspect ratio H/e (a). Strouhal number St_H of the oscillating regime for different aspect ratios (b)

that the frequency f of the global oscillations scales like H/U_j and more generally that H is the relevant length scale for the analysis of the self-sustained global oscillations.

The selected wavelength λ of the impinging jet oscillations is discretised because of the confinement between the jet exit and the impacted wall. The dependency of λ with the impact distance H has the form $H = (n + \epsilon)\lambda$, where the integer n is the cavity mode and ϵ is the correction that takes into account the inlet and outlet boundary conditions ([11] see also [12], and references therein). Visualizations of the central line of the flapping jet (Figure 13) shows that $\epsilon \sim 1/4$ and $n = 1$, at least for $4 < H/e < 14$ (we supect that $n = 2$ above).

5. Discussion

This section is devoted to a tentative explanation of the intrinsic physical mechanisms at the origin of the emerging jet oscillations. More specifically our objective here is to dissect this global instability of the confined impinging flow into basic elements eventually connected via a feedback loop.

We first have checked experimentally that the outflow boundary conditions at the exit of the channel did not modify the dynamics of the flow. Different asymmetries between the top and bottom walls or the lateral boundaries (closed or open) did not affect the observations.

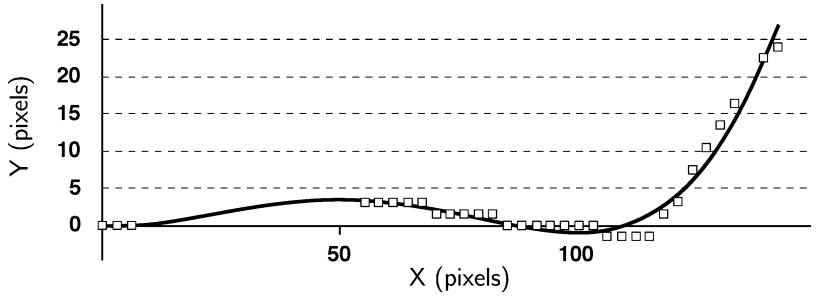

Fig. 13 Experimental determination of the centreline of the flapping jet for $H/e = 7$

We then explored the local dynamics of the three regions described in Martin's classification. The stagnation zone has been first set aside as a trigger for the global oscillations. Following the works of Ho and Nosseir [13] and Tan and Ahuya [14], the edge-tone kind of phenomenons generated by the stretching (and compression) of the vortical structures are not present for the present range of Reynolds numbers (no coherent structures have been observed in the emerging jet), and the Mach number in our experiments is far to weak. Nevertheless this zone certainly takes an active part in the preservation of the self-oscillating regime.

In the following we first discuss the start-up process of the global oscillations on the basis of linear stability analyses of the emerging and wall jets. This study presented in Section 5.1 leads one to suppose that a long-wave sinuous mode of the emerging jet could be receptive to the specific frequencies produced by the natural inflexional instability of the wall jet.

Once settled the global oscillations, the previous linear vision that could explain the onset of the oscillatory regime is no more relevant: the initially driving wall jet is replaced by an unsteady sweeping flow with a completely different structure and a new, nonlinear frequency selection mechanism is to be sought (Section 5.2).

5.1. Onset of the oscillations

The analysis presented here aims at pointing to the driving part of the flow which could possibly trigger the start-up of the oscillations by imposing its frequency, at least during the initial, linear stage of the global oscillations development.

We carried out numerical stability analyses of quasi-parallel basic flows by means of a spectral code [15]. The quantities describing the stability of the flow are classically the wavenumber α and the complex pulsation $\omega = \omega_r + i\omega_i$, which have been non-dimensionnalized with respect to a characteristic length and velocity scale. The mathematical formulation is based on the Orr-Sommerfeld equation and the associated boundary conditions for the normal component of the velocity perturbation. The continuous differential equation is then transformed into an algebraic system after space has been discretized. The numerical code solves the problem by giving the whole spectrum of eigenvalues and the associated eigenmodes.

This protocol is applied to both the emerging and wall jets for different values of the Reynolds number. We rely on the experimental mean velocity profiles below threshold in different sections of the flow in order to define a characteristic base flow (typically at a distance of order e from the jet exit and from the impact respectively for the emerging jet and the wall jet). To carry out the numerical analysis, the experimental data have been fitted by the method of least squares to an exponential fit $\exp(-ax^4 - bx^2)$ for the emerging jet and

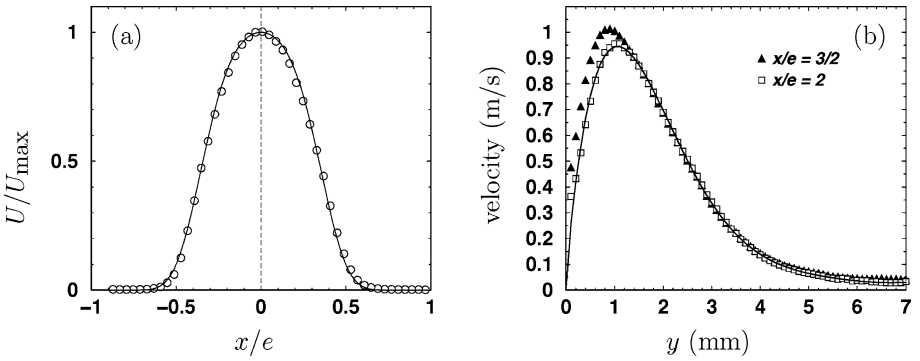

Fig. 14 Non-dimensionalized velocity profile of the impinging jet (a) and dimensional velocity profile of the wall jet at two streamwise locations (b): experimental data (symbols) and associated fits (solid lines)

to a polynomial of order six for the wall jet. These analytical profiles proved to accurately fit the experimental measurements (Figure 14). If the parallel flow assumption is adequate in the case of the emerging jet (see Figure 6 for a qualitative justification), an a priori check can be performed for the wall jet case as shown on Figure 14(b): the non-parallelism of the base flow can be evaluated as $\delta y_m/\delta x$ where δy_m is the variation of the position of the maximum velocity in the wall jet profile (here approximately 0.12 mm) over a streamwise distance δx (here $e/2 = 1.25$ mm). The corresponding ratio is less than 10 percent, which partly justifies the quasi-parallel assumption though it is not completely negligible: for that reason the present stability analysis can only give an estimate in the wall jet case.

5.1.1. Emerging jet

The stability results for $\mathrm{Re}_j = 157$ and 390 around the critical Reynolds number (for $H/e = 8, \mathrm{Re}_j^c \sim 200$) show that the most amplified modes have pulsations ω_r corresponding to dimensional frequencies f always larger than 200 Hz. It is an order of magnitude larger than the characteristic frequencies of the global oscillations observed experimentally, even in their linear start-up. Therefore the natural instability of the emerging jet does not appear to play a dominant role in the triggering of the oscillating regime. The jet is nevertheless unstable to the lower frequencies measured during the onset of the global oscillations, and the corresponding eigenmode has a sinuous structure (data not shown): as a wide-band noise amplifier, the emerging jet could amplify the low frequency perturbations generated by another part of the flow (e.g. the wall jet downstream) and eventually develop large sinuous oscillations that could fuel in return the source of the original fluctuations. This scenario would dynamically close the system and lead to the resonant growth of global oscillations.

5.1.2. Wall jet

The Reynolds number relative to the wall jet is defined as $\mathrm{Re}_w = U_w e_w/\nu$ where U_w and e_w are respectively the maximum velocity and the half height of the wall jet. For the range of Reynolds numbers that we studied, the wall jet is always unstable and the characteristics of the most amplified mode are given in Table 3. The ratio of the phase velocity c_r on U_w and the frequency $f = \omega_r U_w/2\pi e_w$ of the oscillation are also presented. The frequencies are very close to the frequency of the global oscillations, particularly if one notes the sensitivity of

Table 3 Stability of the wall jet

Re_j	Re_w	$\omega_r^{\max}$	$\alpha^{\max}$	$\omega_i^{\max}$	c_r/u_w	f (Hz)
220	175	0.632	1.2	0.04	0.527	17
340	250	0.530	1.15	0.07	0.460	28
480	287	0.480	0.95	0.04	0.505	33

U_w and e_w with respect to the parallel assumption. Depending on the location of the section in the wall jet, these two reference quantities vary and play in the same sense upon f. It has also been observed that the spatial structure of the eigenfunction (data not shown) shows the dominance of the inflexional instability ($y/e_w \sim 0.8$) upon the viscous one ($y/e_w \sim 0.2$) at least for the present range of Reynolds numbers.

On the basis of these results we suspect the wall jet to be at the origin of the low frequency fluctuations that would force the emerging jet dynamics in the early linear stage of the global oscillations evolution. In this vision, the aspect ratio H/e is thought to play a crucial role in the determination of the threshold below which the conjectured resonance is inactive. But a clear explanation of the existence of this threshold is still lacking. For a given aspect ratio H/e, we can just hypothesize the following:

- considering that low Reynolds numbers lead to low frequency instabilities in the wall jet, these low frequencies corresponding to long-wave instability modes for the emerging jet, and
- assuming that the confinement discretizes the large wavelengths of the emerging jet, the largest eligible wavelength being the $n = 1$ cavity mode,

then there should exist a critical Reynolds number below which the wavelengths excited in the emerging jet by the wall jet instabilities are too large to fit in the channel width. The resonance is then deactivated and no global oscillations occur.

5.2. Nonlinear self-sustained oscillations

This section presents a qualitative derivation of the reduced frequency of the self-sustained oscillations once the global instability has nonlinearly saturated.

Self-sustained global oscillations have been found and analyzed in various flows. We can cite works done by Maurel [17] and Bouchet [18] focusing on the case of a jet exhausting in a square cavity as a model for a flowmeter. Villermaux and Hopfinger [19] have shown the presence of global oscillations in the case of multiple interacting jets. In these cases, Landau-type models for the amplitude of the oscillations have been derived.

The core of the analysis applied to the present configuration is to consider that some perturbations are introduced at the jet exit, then convected and amplified. When they reach the obstacle a feedback loop dynamically closes the system [16]. Following Rockwell and Naudascher [12], we considered two hypotheses for the feedback loop:

- the emerging jet reaches the wall and generates coherent structures (vortex dipoles) that produces acoustic waves which are transmitted to the base of the emerging jet at the nozzle exit, or
- the feedback loop is fed by the advection of fluid packets, which assumes the existence of a recirculation flow.

In our experiments, the weak velocities measured outside the emerging jet make the first hypothesis the most plausible.

In that context, as proposed by Rossiter [20], and making use of the experimental observations and the linear stability analysis, we evaluate the period τ of the whole cycle as follows:

$$\tau = \tau_1 + \tau_1' + \tau_2 \tag{3}$$

In Equation (3) $\tau_1 = (1+\alpha)H/c_r$ is the time used by a perturbation introduced at the emerging jet exit to reach the wall. Here $c_r \sim U_j$ is the phase velocity of the jet and $\alpha \sim 1/4$ is the Rossiter deceleration factor in the vicinity of the stagnation point. Similarly $\tau_1' = (1+\alpha)H'/c_r'$ is the estimated formation time of the vortex dipole, with $H' \sim H$ and $c_r' \sim c_r$ respectively denoting the formation length of the dipole from the mean stagnation point, and the phase velocity of the dipole. Finally $\tau_2 \sim H/a$ approximates the return time of the aeroacoustic feedback loop, where a is the sound velocity.

The Strouhal number is then given by

$$\mathrm{St}_H = \frac{H}{\tau U_j} \sim \left[\frac{U_j}{c_r}(1+\alpha)\left(1 + \frac{H'}{H}\frac{U_j}{c_r'}\right) + M_j \right]^{-1} \tag{4}$$

where $M_j = U_j/a$ is the jet Mach number (negligible in the present study). This expression gives a constant Strouhal number $\mathrm{St}_H \sim 0.4$, which is in good agreement with the experimental results.

6. Conclusions

This paper presents experimental results concerning an impinging plane jet in a confined channel. Laser visualizations associated with local velocity measurements put into light the different flow regimes with increasing Reynolds numbers and aspect ratios: stationnary with recirculation zone, local instability of the wall jet then self-sustained oscillations of the whole flow, with ejection of vortex dipoles and sinuous flapping of the emerging jet.

We conjecture the following scenario: in the linear phase, the birth of the global oscillations results from the amplification by the impinging jet of frequencies generated by the inflexional instability of the wall jet. In parallel a wavelength selection occurs depending on the width of the channel. The nonlinear dynamics is closed by an aeroacoustics loop, and the reduced frequency is constant.

In conclusion, the global oscillations of the impinging jet have been characterized for jet Reynolds numbers between 100 and 1000, and aspect ratios from 4 to 9. This phenomenon is crucial with respect to heat transfer and is radically different from the classical wall heat transfer scenarios, with a sweeping of the stagnation point and ejection of vortex dipoles. Therefore such a phenomenon is believed to enhance dramatically the local heat transfer at the location of the impact.

Further theoretical work is under way in order to predict the onset of the oscillations. More particularly, a convective/absolute instability transition for the wall jet could provide with an interesting explanation for the emergence of the self-oscillating regime [21].

References

1. Martin, A.: Heat and mass transfer between impinging gas jets and solid surfaces. Adv. Heat Trans. **13**, 1–60 (1977)
2. Varieras, D.: Etude de l'écoulement et du transfert de chaleur en situation de jet plan confiné. PhD thesis, U. Toulouse III (2000)
3. Beltraos, S., Rajaratnam, N.: Plane turbulent impinging jets. J. Hyd. Res. **1** (1973)
4. Ojha, S.K., Gollakota, S.: Jet impingement on a curved surface. AIAA J. **15** (1977)
5. Striegl, S.A., Diller, T.E.: The effect of entrainment temperature on jet impingement heat transfer. Trans. ASME J. Heat Trans. **106**, 27–33 (1984)
6. Chuang, S.-H.: Numerical simulation of an impinging jet on a flat plate. Int. J. Num. Meth. Fluids **9**, 1413–1426 (1989)
7. AL Sanea, S.: A numerical study of the flow and heat transfer characteristics of an impinging laminar slot jet including crossflow effects. Int. J. Heat Mass Trans. **35**, 2501–2513 (1992)
8. Lin, Z.H., Chou, Y.J., Hung, Y.H.: Heat transfer behaviours of a confined slot jet impingement. Int. J. Heat Mass Trans. **40**, 1095–1107 (1997)
9. Giang, L.S.: Physique et modélisation d'un jet d'impact turbulent. Thèse de l'Institut National Polytechnique de Toulouse, France (1998)
10. Varieras, D., Gervais, P., Giovannini, A., Breton, J. L.: Laser tomographic and interferometric visualizations applied to a confined laminar slot jet impinging on a flat plate. J. Flow Vis. Image Proc. **18**(2), 1–14 (2001)
11. Sarohia, V.: Experimental investigation of oscillations in flows over shallow cavities. AIAA J. **15**(7), 984–991 (1977)
12. Rockwell, D., Naudascher, E.: Self sustained oscillations of impinging free shear layer. Ann. Rev. Fluid Mech. **11**, 67–94 (1979)
13. HO, C.M., Nosseir, N.S.: Dynamics of an impinging jet. Part 1: the feedback phenomenon. J. Fluid Mech. **105**, 119–142 (1981)
14. Tan, C.K.W., Ahuya, K.K.: Theoretical model of discrete tone generation by impinging jets. J. Fluid Mech. **214**, 67–87 (1990)
15. Bottaro, A.: Private communication (1999)
16. Broze, G., Hussain, F.: Nonlinear dynamics of forced transitional jets: periodic and chaotic attractors. J. Fluid Mech. **263**, 93–132 (1994)
17. Maurel, A.: Instabilité d'un jet confiné. PhD thesis, U. Paris VI (1994)
18. Bouchet, G.: Etude expérimentale et numérique des auto-oscillations d'un jet confiné. PhD thesis, U. Paris VI (1996)
19. Villermaux, E., Hopfinger, E.J.: Periodically arranged co-flowing jets. J. Fluid Mech. **263**, 63–92 (1994)
20. Rossiter, J.E.: Wind tunnel experiments in the flow over rectangular cavities. Aeronautical Research Council – Reports and Memoranda **3438**, (1964)
21. Huerre, P., Monkewitz, P.A.: Local and global instabilities in spatially developing flows. Ann. Rev. Fluid Mech. **22**, 473–537 (1990)